AI for Autonomy in Manufacturing

K. Wegener[1,2]

[1]*Institut für Werkzeugmaschinen und Fertigung (IWF) ETH Zürich, CH,*
[2]*inspire AG, Zürich, CH*

INTRODUCTION: With the new paradigms in manufacturing of industrie 4.0 and biological transformation, massive changes will challenge the manufacturing industry and huge benefits will be the recompensation of a successful transformation. Zero fault production, increase of machine autonomy and reliability, increase of quality even for complicated manufacturing tasks with less complexity towards the operator are the goals of this transformation. Complicated processes as for instance additive manufacturing at the border of manufacturability and simplification towards the machine user, leaves only the described development vector.

CONCEPT: The vision "operator integrated" is shown in Fig. 1 for a machine for laser powderbed fusion (LPBF). LPBF is a process that is dominated by a few process parameters, but depends on estimated 200 parameters that are only partly controlled. It is thus the typical complex process, and a generalized CAM-tool as for milling processes does not exist. The concept of biological transformation seeks to find technical solutions by inspiration from biology, by integrating biological elements and by utilizing information technology for an intelligent way of production.

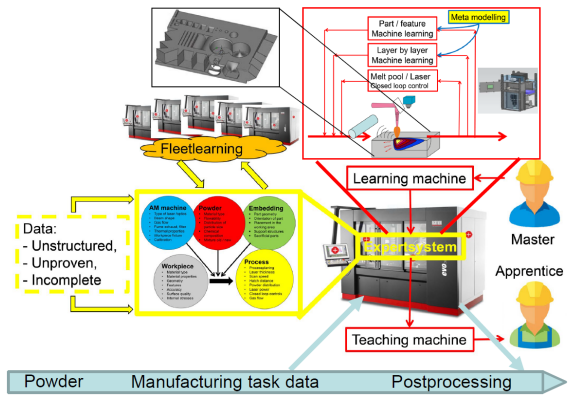

Fig. 1: Vision "operator integrated" as solution for complex manufacturing process additive manufacturing [1].

Similar concepts can be rolled out to actually all manufacturing processes and their machines. Essential is the utilization and integration of diverse bidirectional information streams from and to the manufacturing execution system (MES), other machines, the process, the machine status, and equally important to users with different skill sets. Novelty is the level of monitoring with full field and fused sensors together with intelligent data processing the teaming and communication with human operators and the vault of experience represented by a self-learning expert system on the basis of ontologies.

REALISATION STEPS: Different partial solutions for the concept can be shown as examples: The prerequisite for all data transfer with MES-systems and other machines for federated or transfer learning is the realization of machine connectivity, which is shown for different situations taking also legacy machines into account. Data processing filtering out necessary information is a huge challenge, but the utilization of full field sensors like cameras and microphones enables to delegate this to mathematical processes and surprisingly good monitoring results can be achieved which are far beyond human perceivability. Teaming of humans and machines needs a re-definition of roles and also modifications in the communication concept. The utilization of artificial intelligence (AI) in the entire concept requires the exploitation of different AI tools, namely tools which are adapted to the respective task to be solved. As machines are becoming experts in their manufacturing process by gaining information from skilled operators due to the self-learning and cognitive expert system ethic discussions become necessary. An example of thermal compensation of machines shows the performance gain with the AI application. In addition the benefit of fleet learning is demonstrated for this application.

REFERENCES: [1]Wegener K, Spierings AB, Teti R, Caggiano A, Knüttel D, Staub A (2021). A conceptual vision for a bio-intelligent manufacturing cell for Selective Laser Melting. CIRP Journal of Manufacturing Science and Technology 34: 61–83.

Microstructure of HIPped SLM-Ti6Al4V

E. Brunner[1], J. Wuttig[1], T. Plüss[2], L. D'Antoni[2], CBT. Ly[2], M. de Wild[2]

[1]Sauber Technologies AG, Hinwil, CH, [2]University of Applied Sciences Northwestern Switzerland FHNW, Muttenz, CH

INTRODUCTION: In the Selective Laser Melting (SLM) process, a 3D-object is created layer-by-layer by melting of powder. Its microstructure depends on process parameters [1] and thermo-mechanical post-processes [2]. It is known that the microstructure, especially in the binary titanium alloy Ti6Al4V (3.7165), can be adjusted by hot isostatic pressing (HIP) [3].

METHODS: Ti6Al4V samples for analysis were produced on a MetalFAB-SLM system, see Fig. 1. After a standard stress-release annealing, the samples were hot-isostatic pressed and controlled cooled at various process parameters. Tensile tests were performed according to DIN EN ISO 6892-1. The separated part was used for microstructure examination and etched according to Fuss by Struers. SEM investigations were performed using a Hitachi TM3030Plus system.

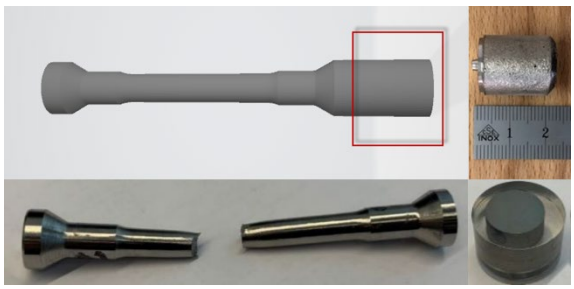

Fig. 1: Tensile tests sample with integrated microsection specimen (red box).

RESULTS: Fig. 2 shows that the microstructure is influenced by the cooling rate. In general, the higher the cooling rate, the finer the microstructure and the lamellar thickness.

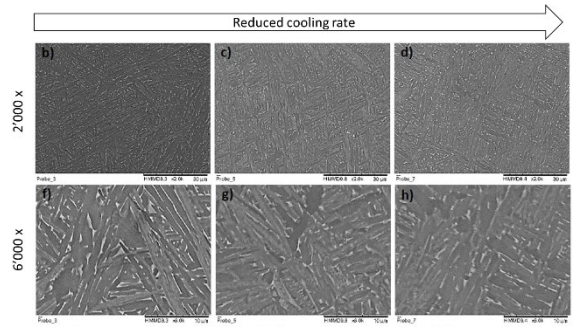

Fig. 2: Microstructure versus cooling rate. Top row magnification 2'000x (scale bar 30 µm), bottom row 6'000x (scale bar 10 µm).

Rapid cooling results in α lamellae and needle-like α'-phase. The α-martensitic phase within the β-phase is only visible after quenching. A higher annealing temperature leads to a coarser microstructure, see Fig. 3 top. As expected, elongation at break increases with decreasing cooling rate and coarser microstructure, while tensile strength and yield strength decrease, see Fig. 3 bottom.

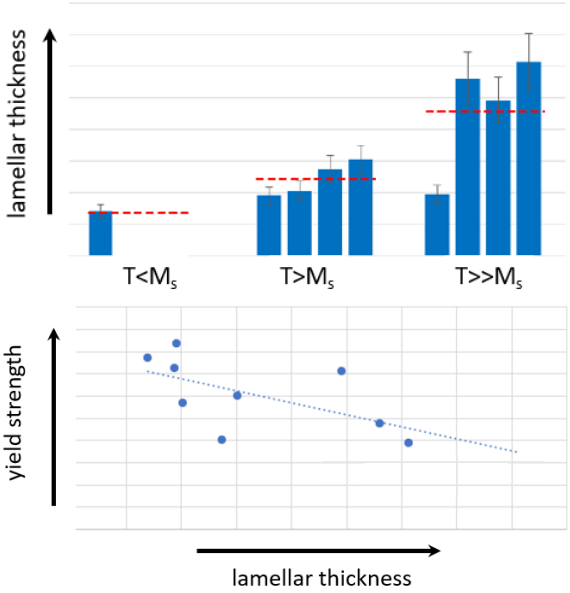

Fig. 3: Influence of hipping temperature on the microstructure (top) and relation between lamella thickness and yield strength (bottom).

DISCUSSION & CONCLUSIONS: It is shown that the microstructure and the mechanical properties of SLM-Ti6Al4V can be optimized to needs by HIP and controlled cooling.

ACKNOWLEDGEMENTS: We would like to thank Struers for etching the samples.

REFERENCES: [1]S. Liu et al., *Additive manufacturing of Ti6Al4V alloy: A review*, Materials & Design, 164, 107552, 2019. [2]A.D. Baghi, *Effective post processing of SLM fabricated Ti-6Al-4V alloy: Machining vs thermal treatment*, J Manuf Proc, 68, Part A, 1031-1046, 2021. [3]Y. Lu et al., *The Influence of heat treatment on the microstructure and properties of HIPped Ti-6Al-4V*, Acta Materialia, 165, 520-527, 2019.

Implants with complex open-pored cellular structure additively manufactured by LPBF using geometry adapted slicing functions

J. Thielsch[1], F. Gebhardt[1], S. Holtzhausen[2], C. Ortmann[3], M. Liebelt[3]

[1]Department of Laser Powder Bed Fusion, Fraunhofer Institute for Machine Tools and Forming Technology, 01187 Dresden, DE, [2]Chair of Virtual Product Development, Technische Universität Dresden, 01062 Dresden, DE, [3]Mathys Orthopaedie GmbH, 07646 Moersdorf, DE

INTRODUCTION: The aim of the work was to improve the dimensional precision of Laser Powder Bed Fusion (LPBF) parts by using suitable exposure strategies and machining parameters. Furthermore, the possibility to avoid costly and time-consuming coating steps for preparation of a complex open-pored cellular structure was investigated for potential implants.

METHODS: The manufacturing of test specimens and implant demonstrator parts was carried out by LPBF. The generation of the cellular structures is based on 3D voxel data. Defined voids are calculated, optimized according to size and subtracted from an envelope geometry. Afterwards, the geometry is analyzed with regard to adapted scan strategies for controlled fabrication of regular and irregular cavities. Preliminary, intermediate and final cleaning was carried out in various cleaning baths with washing solutions including the use of ultrasound and rotation. Compression tests were performed.

RESULTS: Areas with specific topographic features, as e.g. bridges, bulk or open-pored cellular features were automatically identified within the geometric model and assigned with adapted scanning strategies and laser parameters, respectively, using special slicing functions (see Fig.1 and Table 1).

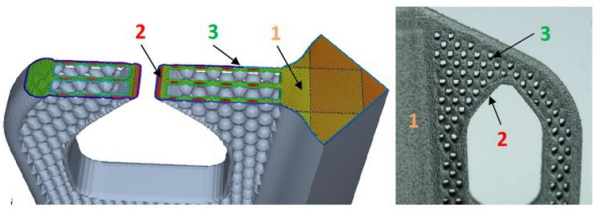

Fig. 1: Cross-section of a shoulder short shaft implant geometry (left) LBPF manufactured shoulder short shaft (right); marked regions are assigned with different LPBF parameters (see Table 1).

Table 1. LPBF parameters for different marked regions in Fig. 1.

Parameter	Laser power / W	Scan speed / mms^{-1}	Laser spot size / µm
1	105	600	100
2	112	700	100
3	100	625	100

A Young's modulus of 4.74 GPa is within the range of comparable osteo implants. Besides it was possible to clean the manufactured components successfully.

DISCUSSION & CONCLUSIONS: This new manufacturing approach resulted in higher dimensional accuracy as well as higher quality of the components (see Fig. 2).

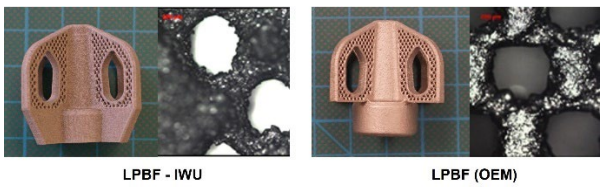

Fig. 2: Fabricated shoulder short shafts based on identical cellular geometry models and corresponding microscope images of cellular structure; LBPF manufactured at Fraunhofer IWU with adapted scan strategies (left) LPBF manufactured at OEM (right).

LPBF fabricated implants with cellular structures offer the potential to support osseointegration without external coatings. Investigations regarding biocompatibility without coating are still pending. In the positive case the production time would be reduced by 6 weeks and the production costs by 33 % compared to the conventional CNC-production route with additional coating step.

ACKNOWLEDGEMENTS: The project "MediSlice" was financially supported by AGENT-3D/BMBF.

Additive manufacturing of zirconia canine resurfacing elbow joint prosthesis via digital light processing

D. Komissarenko[1], T. Graule[1], I. Burda[2], B. Weisse[2], S. Roland[3], B. Seeber[3], D. Koch[4], G. Blugan[1]

[1]Laboratory for High Performance Ceramics, Empa, Dübendorf, CH, [2]Laboratory for Mechanical Systems Engineering, Empa, Dübendorf, CH, [3]Metoxit AG, Thayngen, CH, [4]Kleintierchirurgie AG, Diessenhofen, CH

INTRODUCTION: Elbow dysplasia in dogs is a painful chronic, and potentially degenerative disease that is known to affect certain breeds of dogs, especially larger ones like Labradors, German Shepherds or Rottweilers. The present work aims to develop a ceramic resurfacing implant for dog elbows made by additive manufacturing for less invasive surgery. Digital light processing (DLP) was chosen as an additive manufacturing method to 3D-print the ceramic prosthesis, since it allows to produce the parts with unique design, very high spatial resolution and fine surface finishing. The method is based on the layer-by-layer solidification of a liquid photosensitive resin filled with ceramic powder *via* UV-light exposure followed by debinding of organic components and sintering.

METHODS: The photosensitive ceramic slurries were prepared via incremental addition of the zirconia or alumina powders into a mixture of acrylates and dispersants followed by a planetary ball milling. The solid content of the zirconia and alumina slurries was 35 vol.% and 40 vol.%, respectively. The implants and discs for mechanical testing were 3D-printed using Asiga Pico 2 (Asiga, Australia) and CeraFab 7500 (Lithoz, Austria) printers at different energy doses. The parts were manufactured with the thickness of the layers of 25 microns. The binder system from the parts was removed via thermal treatment at low heating rates. The sintering of the green bodies into dense ceramics was performed in air at 1480 °C for 2 h. The sintered ceramics was characterized via density measurement, SEM, XRD and ball-on-three-balls flexural strength tests.

RESULTS: The present study demonstrates the possibility of 3D-printing high quality zirconia ceramics with relatively low solid content in the slurry via development of a proper formulation, optimization of 3D-printing parameters and design of the debinding and sintering programs. The model of the implant and 3D-printed ceramic implants are presented in Fig. 1.

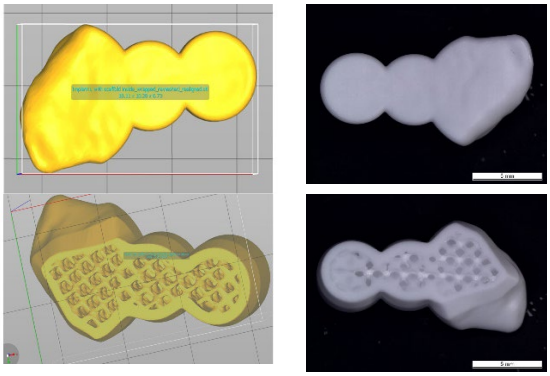

Fig. 1: The model of the implant with scaffold (left), the 3D-printed and sintered ceramics (right).

The density of both zirconia and alumina implants was close to the theoretical one. According to the ball-on-three-balls analysis the average strength of zirconia ceramics was 1566 MPa. The average grains size was 0.5 microns, according to the SEM.

DISCUSSION & CONCLUSIONS: Using 3D-printing, it was possible to manufacture high strength zirconia parts. Different designs of ceramic implants were evaluated for printability. A hydroxyapatite layer was added onto a scaffold part of the implant. Finally, the implantability of the designed implant prototypes was verified using cadavers of dogs.

ACKNOWLEDGEMENTS: The research was sponsored by the Innosuisse project ReSurf (Application number 39644.1).

Wireless Power Transfer for "Smart" Implants

S. Bauer, W. Döll, D. Ulrich

Helbling Technik Bern AG, Liebefeld-Bern, CH

INTRODUCTION: Several technologies for wireless power transfer are already available to developers of medical devices. The spectrum of electromagnetic solutions ranges from the low-frequency kHz to the high-frequency GHz range. On an example of an eye implant, we show which technologies for wireless power transfer are available today and how the most suitable one can be chosen.

METHODS: For the development of the wireless power transfer solution, we used simulation methods as well as testing in the high-frequency laboratory. For the simulation, a combination of self-developed and commercial simulation tools came into use to precisely represent the electromagnetic boundary conditions, including absorption in the surrounding tissue.

RESULTS: We developed a wireless power link for an electronic eye implant for continuous measurement of the intraocular pressure. Simulations showed that two variants were possible: a conventional solution in the near field using magnetic coupling at 13.56 MHz, and a solution in the far field at 900 MHz.

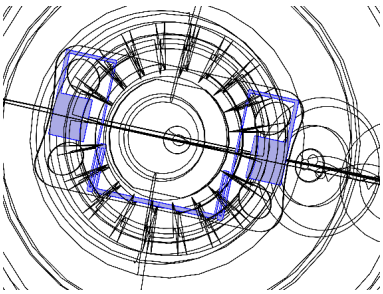

Fig. 1: Intra-ocular lens with antenna (in blue), simulation model of an anatomical eye.

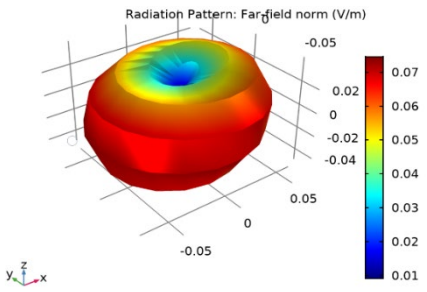

Fig. 2: Radiation characteristics of the Ultra High-Frequency antenna (simulation result).

A pre-clinical study with implants operating in the near field at 13.56 MHz was successfully completed and in-vitro testing confirmed the simulation results, which indicated a range of up to 1 m for wireless power transfer at 900 MHz. But there was another argument in favor of the latter solution: Because of the dielectric properties of the surrounding tissue, a UHF antenna at 900 MHz can be implemented with significantly smaller dimensions than an antenna in air. With proper design methods, it was even possible to place the antenna on the non-optical surface of an intraocular lens.

DISCUSSION & CONCLUSIONS: Over the past few years, we have developed various wireless power and data links for medical applications that work in the frequency range from 10 kHz to 2.5 GHz. Depending on the area of application, standard technologies such as NFC (13.56 MHz) or Bluetooth (2.4 GHz) can be employed. However, if the application-specific needs cannot be met with standard technologies, proprietary developments are used to close this gap.

In orthopaedics and other surgical fields wireless power transfer to implants might become more and more important. "Smart" implants such as the Zimmer Persona IQ© equipped with sensing and wireless data communication capabilities might need external power charging, as new functionalities will be added. Smart implants will have the potential to support the shift towards a more predictive, data driven health care approach.

REFERENCES: Khan, S.R.; Pavuluri, S.K.; Cummins, G.; Desmulliez, M.P.Y. Wireless Power Transfer Techniques for Implantable Medical Devices: A Review. Sensors 2020, 20, 3487.

H.-J. Kim, H. Hirayama, S. Kim, K. J. Han, R. Zhang and J. -W. Choi. Review of Near-Field Wireless Power and Communication for Biomedical Applications. In IEEE Access, vol. 5, pp. 21264-21285, 2017.

Surface treatments of 3D printed Nitinol stents

L. Jerjen[1], B. Schnyder[1], T. Journot[2], O. Banakh[2], J. Pralong[1], S. Rey-Mermet[1]

[1]School of Engineering, HES-SO Valais, Sion, CH, [2]HE-Arc, Neuchâtel, CH

INTRODUCTION: Above its austenitic/ martensitic transition temperature (TT), Nitinol is superelastic and below it has shape memory capacity. If TT is below the body temperature, the stent can be cooled and deformed to reduce its diameter before being inserted in the arteria. It will then recover its expanded geometry. Stents are currently produced by laser cutting or welding of Nitinol tubes or wires. In this work, stents are 3D printed by Selective Laser Melting (SLM).

METHODS: Stents have been printed by SLM with an SLM Solutions 125 printer by using an atomized Nitinol powder with a Dv50 of 35 µm and a composition of 50.8 at% of nickel. Printing parameters have been varied to adapt A_F that was measured by Differential Scanning Calorimetry on lattice structures. The minimal "wire" diameter obtained as printed was of 200 µm.

The stent surface has been treated by electropolishing (EP) to reduce its roughness. Two stainless steel 3D printed meshes, having the same patterns as the Nitinol stents have been used as outer and inner counter-electrodes. A parametric study has been performed to establish EP conditions: electrolyte molar ratios of KCl:ethylene glycol between 1 to 5 %, temperature of 80 °C or 130 °C with an applied voltage of 60 V.

After polishing, some stents have been coated by a 50 nm thick TiO_2 layer by Atomic Layer Deposition or by a 1 µm thick Tantalum layer sputtered by Physical Vapour Deposition.

Cytotoxicity in L929 cell cultures and hemocompatibility by osmotic fragility assay have been performed on as-printed, polished and coated stents according to ISO 10993-12 guidelines.

RESULTS: By varying the energy density between 73 and 250 J/mm^3 and power from 50 to 250 W, it has been possible to control A_F between 27 °C and 98 °C in the stents. The stents have a wire diameter of approximately 200 µm before EP.

EP helps to reduce surface roughness to 13 nm (ISO 21920) on flat samples. For 3D structures polishing, stainless steel inner and outer counter electrodes have been printed by SLM. It has permitted to reduce the roughness significantly on the outside and the inside of the stents as shown on figure 1.

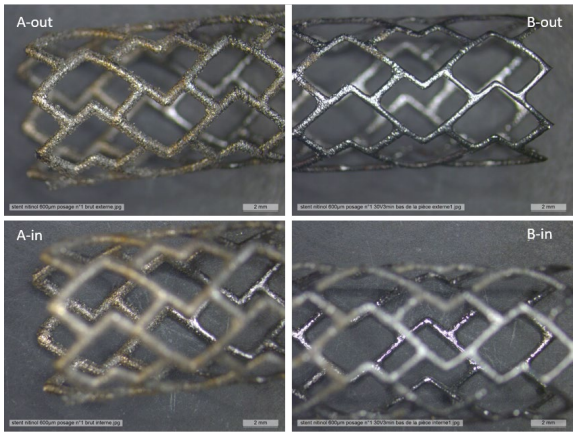

Fig. 1: A-out and A-in: outside and inside view of the mesh roughness as printed. B-out and B-in same views after EP

A mechanical deformation corresponding to a diameter contraction by a factor 4 has been successfully recovered by heating the stent up to 35 °C in hot water. Fatigue tests in radial compression have been realized on a specifically constructed setup. Stents survive at least 10^5 cycles with a radial deformation of 1%.

Cytotoxicity test have shown that all the 3 samples are bio- and hemocompatible. However, TiO_2 coating seems to significantly reduce the loss of red blood cells.

DISCUSSION & CONCLUSIONS: Stents with adequate mechanical and physical properties have been successfully printed by adapting SLM parameters and electropolished to reduce their inner and outer roughness. SLM has the advantage of reducing the number of processing steps and of allowing more geometry freedom. As printed, polished and TiO_2 coated stents are biocompatible and hemocompatible.

ACKNOWLEDGEMENTS: The authors want to acknowledge the University of Applied Sciences and Arts Western Switzerland (HESSO) for funding.

Micro-arc anodized magnesium AZ31 alloy: towards application in veterinary implants

O. Banakh[1], T. Journot[1], Y. Savary[1], A. Hämmerli[2], J.-C. Puippe[3]

[1]Haute Ecole Arc Ingénierie (HE-Arc), La Chaux-de-Fonds, CH,
[2]Kyon AG, Zurich, CH, [3]Steiger Galvanotechnique SA, Châtel-St.-Denis, CH

INTRODUCTION: Mg-based alloys can be used as biodegradable materials in cardiovascular and orthopedic implants. The aim of this study was to evaluate the AZ31 alloy for its use in veterinary implants. As the alloy is very sensitive to corrosion in biological medium, Plasma Electrolytic Oxidation (PEO) surface treatment has been applied to the implant to provide its mechanical integrity in the body over several months by slowing down the corrosion process.

METHODS: AZ31 implants (25 mm diam.) were produced by machining according to the design in Fig. 1 and post-finished by vibro-abrasion. PEO surface treatment was performed using a CIRTEM® bipolar pulsed current source (f=500 Hz; J+= 24÷64 A/dm^2). The electrolyte used was a mixture of 2.8 g/l NaOH and 7.5 ml/l Na_2SiO_3 (pH=12.5). Treatment time was 5 min. The surface and cross-section morphology of the treated samples were examined by Scanning Electron Microscopy (SEM) and optical microscopy. Corrosion degradation tests were performed by immersing the samples in a simulated body fluid (SBF, Ringer solution) at 37 °C during 40 days. For some samples, hydrogen gas release was also measured. Mechanical tests were performed on the PEO-treated implants before and after several weeks of immersion in a SBF solution. The test consisted of applying a progressive force perpendicular to the surface of the implant. During the test, the applied force and the displacement of the implant were recorded.

RESULTS: The current density used in PEO process shows an influence on the surface morphology of the anodized layer. The PEO layer exhibits the pores ranging from 5 to 10 µm in diameter as well as the cracks, usually obtained by this process. The layer is homogeneous in thickness over the entire implant geometry. Metallographic tests showed an anodized layer thickness of about 10-15 µm. The chemical EDX analysis showed mainly Mg and O peaks confirming the presence of oxidized magnesium. The influence of current density on the corrosion resistance of the implants is less significant. Potentiodynamic tests showed a decrease in the corrosion current of PEO-treated parts by a factor of 700 as compared to untreated AZ31 samples.

The mechanical strength of PEO-treated implants is satisfactory. The coating slightly affects the mechanical strength of the implant, decreasing the force required to bend the implant 2 mm by 40 N. The mechanical strength of the implant decreases as the implant degrades. After 5 weeks immersed in SBF, the force required to bend the implant 2 mm dropped from 700 N to 600 N (Fig. 2).

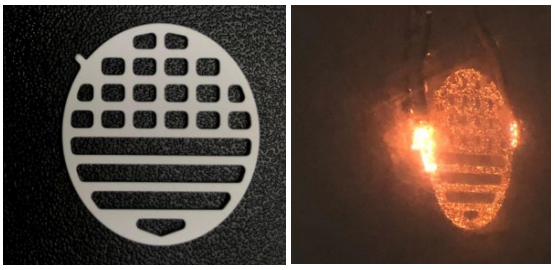

Fig. 1: The prototype implants: before (left) and during PEO treatment (right).

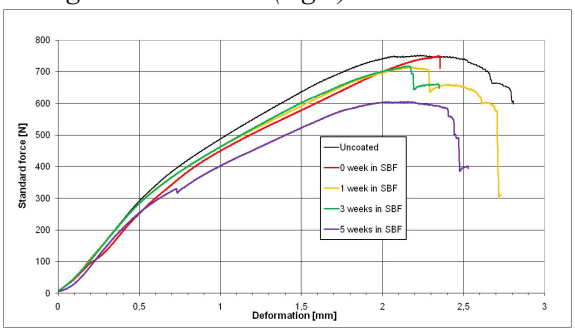

Fig. 2: Mechanical tests performed on the untreated (black curve) and PEO treated implants after their immersion into SBF solution up to 5 weeks.

DISCUSSION & CONCLUSIONS: PEO treatment has significantly improved the corrosion resistance of AZ31. Mechanical tests showed good mechanical stability of the treated implants after their immersion in SBF for 5 weeks.

ACKNOWLEDGEMENTS: C. Csefalvay (HE-Arc) is acknowledged for the SEM-EDX investigations.

Anti-bacterial coating for implant surfaces based on electrochemically-formed calcium hydroxide

H. Holeczek[1], O. Braissant[2], J. Rüegg[3], M. de Wild[3]

[1]Medicoat AG, Mägenwil, CH, [2]University of Basel, Allschwil, CH, [3]University of Applied Sciences and Arts Northwestern Switzerland, Muttenz, CH

INTRODUCTION: Increasing numbers of cases with infection after implant operation drive the demand for an anti-bacterial property of the implant surface. Such a bactericidal effect should be strong enough to kill bacteria that might reach the implant surface during or after the surgical procedure. On the other hand, it should not affect the body of the patient with possible long-term effects.

METHODS: Titanium disks and screws have been coated with a rough titanium layer by thermal plasma spray coating first. Samples were then coated with a compound layer of $Ca(OH)_2$. The surface of the coated samples was then moistened with LB medium containing *S. epidermidis* and *S. aureus* with a concentration of 10^5 CFU ml^{-1}. Samples were then placed in a micro-calorimeter.

RESULTS: Activity of the bacteria was measured indirectly via the produced metabolic heat. The diagram resulting from Gompertz curve fitting (Fig. 1) shows the reduced metabolic heat for the $Ca(OH)_2$ coated sample.

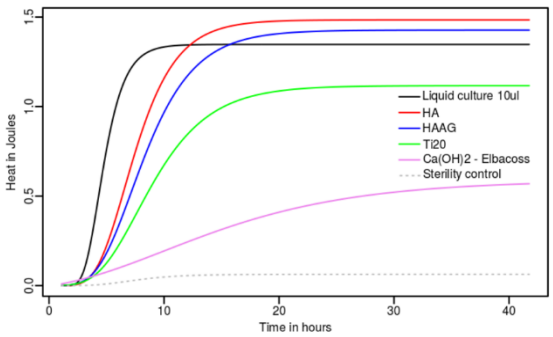

Figure 1: Modelled data from Gompertz curve fitting of micro-calorimeter measurements.

The growth rates of the different populations (Fig. 2) were calculated from the measurement data and show a considerably reduced growth on the samples with anti-bacterial $Ca(OH)_2$-coating, compared to those with hydroxyapatite (HA) or pure titanium (Ti20).

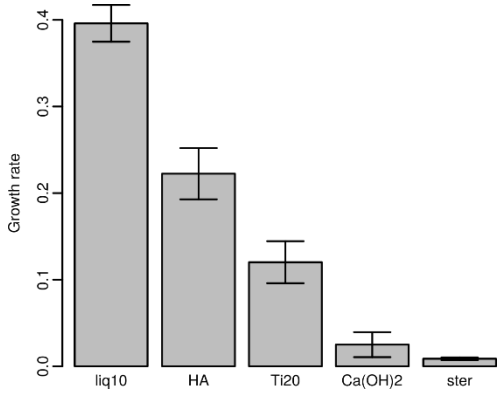

Figure 2: Growth rates computed from calorimeter data.

DISCUSSION & CONCLUSIONS: Measurements with a micro-calorimeter have been used to indirectly detect the bacterial metabolism activity by measuring the heat generated. On samples coated with $Ca(OH)_2$ a significant reduction of bacterial activity was detected which points to greatly reduced growth of the initial organisms. Thus, the anti-bacterial effect of such a coating has been shown.
As the coating consists only of Ca and hydroxyl ions, which are both completely resorbed by the body, the active coating is removed after some time. The contact-killing effect is only active directly on the surface of the coated specimen. Yet, there is no risk of long-term effects to be expected when the coating is used in the body. Furthermore, our in-vivo study showed good osseointegration of coated implants in rats [1].

ACKNOWLEDGEMENTS: The authors would like to thank the Forschungsfonds Aargau for supporting the project 20140331_07_Z _ELBACOSS.

REFERENCES:

[1]N. Harrasser, M. de Wild, J. Gorkotte, A. Obermaier, S. Feihl, M. Straub, R. von Eisenhart-Rothe, H. Gollwitzer, J. Rüegg, W. Moser, Ph. Gruner, R. Burgkart, *Evaluation of calcium dihydroxide- and silver-coated implants in the rat tibia*, J Appl Biomater Funct Mater 14(4): e441-e448 (2016).

Artificially induced peri-implant inflammation around mechanically loaded Zirconia and Titanium implants.

S. Wolf[1], CM. Sprecher[2], S. Milz[3], H. Woelfler[4], M. Gahlert[1], S. Janner[5], B. Meng[6], DL. Cochran[6], S. Roehling[1]

[1]University of Basel, CH, [2]AO Research Institute, Davos, CH, [3]University of Munich, DE, [4]University of Bamberg, DE, [5]University of Berne, CH, [6]University of Texas, USA

INTRODUCTION: The present study aims to investigate the influence of an implant material on the mineralized tissue response in artificially induced peri-implant inflammation and infection around the upper part of mechanically loaded dental implants.

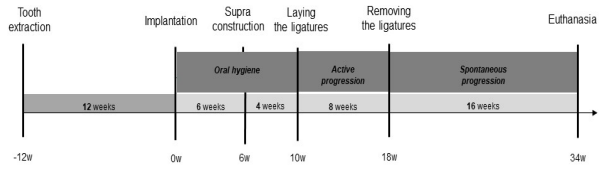

Fig. 1: Timeline illustrating the different phases of the study.

METHODS: Five male dogs (American Foxhound) received 4 implants (Titanium or Zirconia, randomly assigned position, micro-rough surface topography) on each side of the jaw. The implants were placed in preconditioned bone with the original teeth removed 12 weeks before implantation (Fig. 1). After installation of the load bearing supra construction, ligatures around the implant neck were installed to induce local inflammation. Eight weeks later ligatures were removed and 16 weeks later animals were euthanized and bone/implant blocks (including the gingiva layer) were obtained.

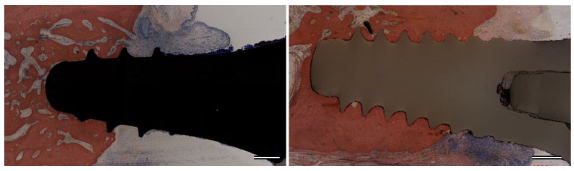

Fig. 2: Histological images of Titanium (left) and Zirconia (right) implant sections stained with Giemsa Eosin. Scale bars: 1000 µm.

After preparation of resin embedded Giemsa/Eosin-stained sections (Fig. 2), peri-implant bone density and peri-implant contact ratio and bone loss of the alveolar crest were histomorphometrically determined in a buco-lingual plane.

RESULTS: Bone resorption around Titanium implants was significantly increased compared to Zirconia implants. The effect was most pronounced on the lingual side (Fig. 3). Other parameters did not show significant differences. All implants clinically appeared to be stable.

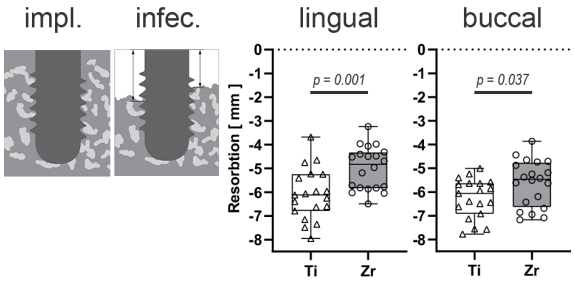

Fig. 3: Significantly increased bone resorption around Titanium implants compared to Zirconia implants, especially at the lingual side. The schematic illustrations show bone around the implant after implantation (impl.) and after continuous inflammation and accompanying infection (infec.).

DISCUSSION & CONCLUSIONS: Mechanically loaded Zirconia implants exhibited significantly reduced peri-implant bone loss at the end of a 16 week healing phase after artificially, ligature-induced inflammation, when compared to Titanium implants with a comparable surface topography and roughness. The histological results are in line with radiological results, already published in the literature [1].

ACKNOWLEDGEMENTS: This study was supported by ITI-Grant Number 920_2013.

REFERENCES:

[1]Stefan Roehling et al; Int J Oral Maxillofac Implants 2019:357–365.

Clinical Applications of Patient-Specific Implants: How to Avoid Reinventing the Wheel

H. Yau[1], EWF. Yau[1], C. Fang[2,3], CHB. Yung[1]

[1]KOLN3D Technology SA, Geneva, CH, [2]The University of Hong Kong

INTRODUCTION: Patient-Specific Implants (PSI) have been demonstrated to have potential in significantly improving patient outcomes and post-operative quality of life. However, there are unavoidable risks associated with the use of a bespoke product during a surgical procedure that often strays from standard procedure and requires specific attention. Hence it is imperative that the scope of application regarding patient-specific implants be flexibly determined on a case-by-case basis to mitigate unnecessary risk exposure [1], [2].

METHODS: Patient-specific implants were planned, designed, fabricated, tested, and surgically implanted by a surgeon-lead collaborative team between the University of Hong Kong and KOLN3D Technology. Extent of implant customization was adapted for case specifics and needs. Cases were and will be followed up for up to a year post-op to evaluate efficacy of PSI.

RESULTS: Three case studies will be shared as examples of varying extents of application by patient specific implants within the greater surgical context. The first case is that of a hip replacement resulting from a tumor resection that utilizes a patient-specific hip reconstruction that is affixed to a commercial acetabulum cup/femoral stem (Fig. 1). The second case is a temporomandibular joint replacement employing a patient-specific mandible component and a commercial UHMWPE temporal bone component.

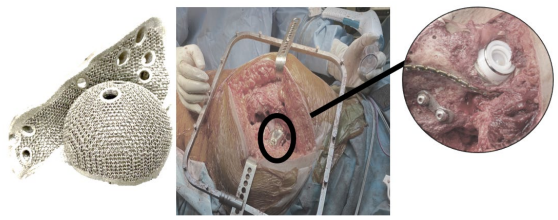

Fig. 1: Hip Reconstruction PSI with commercial acetabulum cup and femoral stem.

The third case is a talar replacement completely bespoke (Fig. 2), with osteoinductive features to promote improved biological integration.

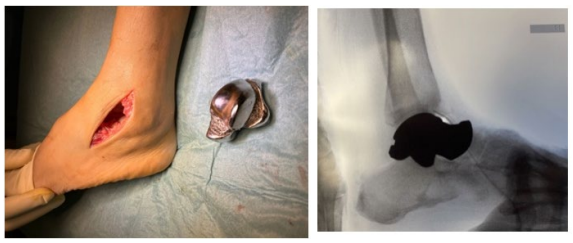

Fig. 2: Bespoke Talar Replacement Implant.

DISCUSSION & CONCLUSIONS: All surgeries were completed without complication. No surgical revisions associated with implant failure were required.
By identifying benefits of patient-specific implants and utilizing standardized products where possible, Health and Quality of Life improvements to the patient are maximized whilst risk exposure is controlled.

ACKNOWLEDGEMENTS: All PSI clinical cases were completed as a collective effort with Hong Kong public hospitals and respective surgeons under liaison through and support from Dr. Christian Fang of The University of Hong Kong.

REFERENCES: [1]Y.N. Chim, S.K.H. Chow, S.Y. Mak, M.M.C. Li, B.C.H. Yung, E.W.F. Yau, C.S. CHUI. (2020) 3D-printed cobalt-chromium porous metal implants showed enhanced bone-implant interface and bone in-growth in a rabbit epiphyseal bone defect model. Bone Reports. 13. 100375. 10.1016/j.bonr.2020.100375.
[2]C. Fang, H. Cai, E. Kuong, C.S. CHUI, Y. Y.C. Siu, T. Ji, I. Drstvensek (2019) Surgical applications of three-dimensional printing in the pelvis and acetabulum: from models and tools to implants. Der Unfallchirurg. 122. 10.1007/s00113-019-0626-8.

Challenges and *in-vitro* solutions for the biocompatibility assessment with chemical characterization based on ISO 10993

S. Savic, S. Weissensteiner, D. Neubert, E. Mertl

OFI – Austrian Research Institute for Chemistry and Technology, Vienna, AT

INTRODUCTION: The biocompatibility assessment of medical devices is regulated in the MDR, not specifying how this information shall be retrieved. The ISO 10993 series is therefore THE regulative tool routinely applied for the biocompatibility assessment of medical devices. By categorizing products by contact (blood, mucosa, intact skin) or duration, different endpoints or hazards need to be tested. The hazards addressed in ISO 10993 can be assessed step by step. However, considering the list for a hip implant, eleven endpoints would need to be evaluated. This can quickly become a very expensive task. Alternatively, a chemical characterization is the first step. Substances that are found in the system can further be identified and risk assessed based on substance information and amount.

For the extraction, the ISO serves as guideline and sets extraction conditions, however, here some problems may occur. As the solvents tend to overestimate the conditions present in the human body and are way too harsh, samples are often damaged. Here the question arises in how far the chosen conditions reflect the true nature of the application.

If during the identification unknown substances remain, these knowledge gaps can be overcome by using alternative *in-vitro* methods.

METHODS:

Chemical Characterization: Due to chemical differences (polarity, organic/ inorganic; metals, etc.) a complete characterization requires three different methods. These are the HPLC-MS system, a GC-MS system and the ICP.

In – vitro tests: Cytotoxicity is determined using L929 Cells and exposing a samples' extract in cell culture medium for 24 h to the cells. Sensitization is done with an MDA-ARE cell line, that upon the exposure of potentially sensitizing substances activates the ARE-Nrf2 pathway that later can be visualized. The second test for sensitizing potential is the *in-chemico* DPRA assay, where the potency of a sample extract to bind to amino acids Lysine and Cysteine is estimated. The test for irritation is based on human skin models where extracts are exposed to for 18 h.

RESULTS: In case no complete characterization of the detected substances is possible, the various *in-vitro* and *in-chemico* assays can provide suitable additive information of the different hazards. For the case that everything is well characterized but no literature on these substances can be found, the tests are also serving their necessity as certain hazards can be excluded.

The second problem is depicted in Figure 1 showing an experimental extraction of samples with different solvents. The advantage is that weaker solvents mimic the human body more realistically and are compatible with skin models or cell cultures whilst not damaging the sample. On the other hand, for hazard identification worst-case solvents are required.

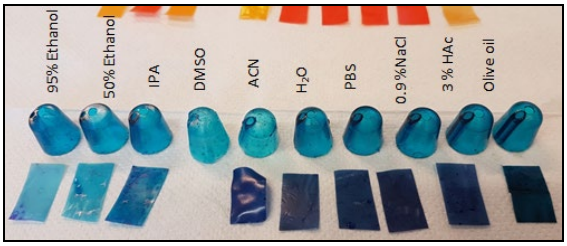

Fig. 1: Effect of different solvents on the same sample in plane and moulded form.

DISCUSSION & CONCLUSIONS: In a case study all substances identified could be risk assessed, resulting in no need for further *in-vitro* tests. For the case that a sample is obviously damaged the extraction conditions can be altered and solvents diluted to prevent damage, but no complete shift will be possible. Animal free alternative tests are a great additional tool to on one hand complete the picture and on the other use solvents that reflect more realistic conditions. Nevertheless, the problem of extracting unrealistically too much by exaggerated conditions remains an issue of argumentation in the report.

ACKNOWLEDGEMENTS: This research is done at the OFI by the department for medical devices and the chromatographical analysis.

In vitro testing of degradable magnesium implants – Avoiding the pitfalls

H. Schmotzer[1] and S. Rogge[2]

[1]SigmaRC GmbH, Cham, CH, [2]botiss biomaterials GmbH, Berlin, DE

INTRODUCTION: Biodegradable magnesium (Mg) implants have been introduced in orthopaedic and vascular surgery over the last decade. Most recently, implants for oral regenerative applications have been added. Mg and its alloys combine good mechanical properties, excellent biocompatibility, and the ability to degrade in a reasonable time period.
Extensive preclinical testing is required for regulatory submission. Commonly, test strategies follow established pathways based on pertinent standards and regulations, which have been developed and validated using inert devices. Testing laboratories obtain accreditation tests built on these standards.
In vitro testing of biodegradable Mg using established methods presents an extra challenge as the break-down is by corrosion which is a chemical reaction between the implant and its surrounding. Hydrogen development during degradation is a well-known phenomenon.
In the following, examples are provided, how this may lead to false-negative results when established protocols are used.

Example 1: Magnesium based products may come into contact with various substances during manufacturing. Here, a nitric acid containing solution was used for surface finish. After extraction of the finished device the residual contamination by nitrates (NO_3^-) was below the detection limit. After packaging and accelerated aging @ 60 °C black stains occurred. Samples were sent for ToF-SIMS analysis comparing stained and unstained regions. Dark zones showed only a mild signal intensity for nitrates; however, a strong signal was measured for nitrites (NO_2^-) suggesting that the nitrates had been reduced by the Mg. XPS analysis of such regions demonstrated a complete absence of metallic Mg. All Mg was in the oxidised state. In contrast, unstrained regions showed approximately 20% metallic Mg.

Example 2: During final cleaning, medical devices are commonly rinsed in EtOH or IPA to replace the water and accelerate drying.
Mg is rather soft and may easily be scratched even when using polymeric tools. Metallic Mg sheets were mildly scratched and suspended in EtOH. After drying, packaging and accelerated aging @ 60 °C the scratches turned dark grey to black. ToF-SIMS analysis demonstrated oxidised Mg in the dark markings as well as short, oxygenated hydrocarbons suggesting the formation of ethanolates in the scratches which were reduced during ageing.

Example 3: Particle burden on medical devices is determined as part of the validation of the cleaning process (ISO 19227, ASTM F3127). Commonly, particles are determined using the water-based extracts for TOC (ASTM F2459). However, depending on the type of alloy and surface treatment, corrosive processes during extraction may start to release particulates. Device testing resulted in a residual particle burden of 77.7±8.3 µg/sample which would have been well above the specific acceptance level. After rinsing the filters with 5% nitric acid, the particle burden was below the detection limit of 17 µg/sample.

Example 4: Similarly, suspended corrosion products may influence pH and osmolarity of extracts when conducting cytotoxicity testing according to ISO 10993-5 if unfiltered or uncentrifuged extracts are used. The individual corrosion rate of a given alloy influences Mg concentration, pH and osmolarity as demonstrated by Fischer et al. [1].

DISCUSSION & CONCLUSIONS: Mg is highly reactive directly affecting its immediate environment unlike other already established biodegradable materials which generally break down by dissolution or hydrolysis. This needs to be assessed during the creation of a test plan for preclinical studies prior to actually starting them. Controlled and documented deviations from the standard laboratory procedures may be necessary to avoid undue rejection of a material or device.

ACKNOWLEDGEMENTS: This work was supported by botiss biomaterials GmbH, Berlin.

REFERENCES: [1]Fischer et al. (2011) Improved cytotoxicity testing of magnesium materials. Materials Science and Engineering: B; Volume 176, Issue 11, 830-834.